Optics Letters

Spontaneous generation of orbital angular momentum crystals using a monolithic Nd:YAG nonplanar ring laser

Guoping Lin,[1,*] Yaqin Cao,[1] Zehuang Lu,[1] and Yanne K. Chembo[2]

[1]MOE Key Laboratory of Fundamental Physical Quantities Measurement, Hubei Key Laboratory of Gravitation and Quantum Physics, PGMF and School of Physics, Huazhong University of Science and Technology, Wuhan 430074, China
[2]Georgia Tech—CNRS Joint International Laboratory [UMI 2958], Atlanta Mirror Site, School of Electrical and Computer Engineering, 777 Atlantic Dr. NW, Atlanta, Georgia 30332, USA
*Corresponding author: guoping_lin@hust.edu.cn

Received 1 November 2018; revised 29 November 2018; accepted 30 November 2018; posted 4 December 2018 (Doc. ID 349913); published 2 January 2019

We report the emission of localized orbital angular momentum (OAM) crystals in a millimeter-size monolithic Nd:YAG nonplanar ring laser. Narrow-linewidth single-frequency lasing in the kilohertz level featuring crystal-like vortices is obtained via phase locking of Laguerre-Gaussian modes in the cavity. It is found that the spatially degenerate OAM of high-order LG modes can be easily broken by superimposing a low-order mode, leading to crystal-like vortices. Our theoretical analysis is found to be in agreement with the experimental results for both intensity and interference patterns.

https://doi.org/10.1364/OL.44.000203

Vortex formation has been extensively investigated in various fields of physics, including Bose–Einstein condensate (BEC), superconductivity, and superfluidity. This phenomenon also exists in optics and is generally referred to as helically phased beams [1–3]. The spiral phase of the simplest vortex laser at its waist can be expressed by $\exp(i\ell\phi)$ with ℓ being the topological charge or handedness, and ϕ being the azimuthal angle. Its intensity profile turns out to be doughnut-shaped with zero intensity at the phase singularity point upon propagation. Interestingly, vortex lasers were also found to carry the orbital angular momentum (OAM) equivalent to $\ell\hbar$ [4], and a significant body of scientific literature has been devoted to this field. Fundamental research has been extensive in the area of nonlinear and quantum photonics [5–13]. Many applications using vortex laser beams have also been demonstrated so far such as super-resolution microscopy [14], optical trapping and manipulation [15,16], high-precision laser micromachining [17,18], and high-capacity optical communication [19,20].

Various approaches based on dielectric and metallic materials have been developed to generate such vortex laser beams. For instance, one can use diffractive and phased optical elements, the reorientational nonlinearities in the liquid crystals, or employ optical mode converters, either internal or external to the laser cavity [21–34]. On the other hand, the direct generation of vortex lasers has also been reported in optical oscillators by selectively exciting Laguerre–Gaussian (LG) modes without the need of external optical elements [35–41]. In particular, kilohertz-level narrow-linewidth LG_{01} vortex continuous lasing was observed in a solid-state monolithic nonplanar ring oscillator (NPRO) [41]. The rigidity and performance of NPROs have been verified in ground and space projects related to the measurements of gravity and gravitational waves [42–44].

Similar to vortex formation in BECs and other quantum systems [45,46], the material-like behavior of optical vortices or optical OAMs can also be observed. For example, phase- and amplitude-locked vortex crystals exhibiting single-frequency characteristics have been reported in vertical-cavity surface-emitting semiconductor lasers [38]. Note that similar vortex pairs featuring the so-called circling vortices have been observed previously in four-mirror- based ring cavities containing a photorefractive nonlinear element [36,37]. More recently, a four-mirror-based nonplanar ring resonator has also been employed to create synthetic Landau levels for photons [12].

Here we demonstrate for the first time, to the best of our knowledge, the direct generation of optical OAM crystal lasers with a monolithic nonplanar ring laser. Both intensity distribution patterns and interferograms have been experimentally obtained, and display a good agreement with the theoretical results based on phase-locked LG modes. For instance, we find that the degeneracy of multiple OAMs of high-order LG modes in space can be broken by super-imposing a phase-locked LG_{00} beam. The resultant optical OAM crystal pattern shows spatially distributed vortices of single OAMs. Benefiting from the advantages of monolithic NPRO, OAM crystal lasers are found to feature kilohertz-level linewidth performance.

The optical OAM crystals were studied in a solid-state monolithic laser based on an Nd:YAG NPRO, as illustrated in Fig. 1(a). In comparison to whispering-gallery mode resonators which use continuous total internal reflections [47–49], NPROs use only a few TIRs and a coated high-reflection surface for efficient free-space coupling. Here the optical round-trip at a lasing wavelength of 1064 nm of the NPRO

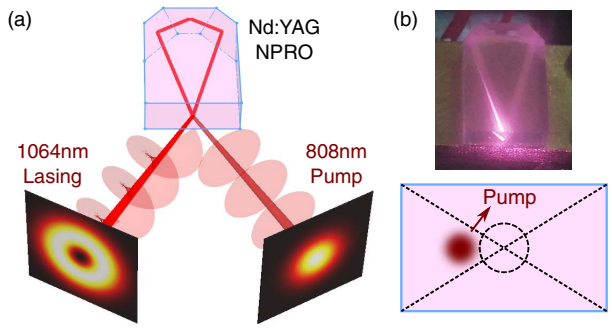

Fig. 1. (a) Schematic of a monolithic vortex laser based on an Nd:YAG NPRO pumped by a fundamental Gaussian beam at 808 nm. (b) Top, a photo of the Nd:YAG NPRO taken while the vortex laser is on operation; bottom, an illustration of the off-axis pumping scheme on the coated surface of the NPRO.

was formed by three TIRs and a high-reflection surface. Such structures are well known for generating very narrow-linewidth single-frequency lasers [50].

Figure 1(b) shows a photograph of the Nd:YAG crystal when vortex lasing was generated. The dimensions of the crystal are $3 \times 8 \times 12$ mm^3, and the doping concentration is 0.8%. The optical path of the laser beam can be clearly visualized by the pink rays. The decaying brightness of the beam is a result of absorption and diffusion inside the crystal. The angle of incidence at the coated surface was about 30 degrees. Also shown is an illustration of the off-axis pumping scheme. The Gaussian pump laser was focused off-center at the coated surface of the NPRO to establish LG mode lasing [41], which can also be observed in the photography of the NPRO. The output laser beam at 1064 nm was split into three beams for laser characterization. The first one was directed to the scanning Fabry–Perot interferometer (SFPI) for monitoring the single-frequency lasing behavior. The second one was used to examine the topological charges of the vortex lasing beam using a simple interferometric method described in Ref. [41]. The last output beam was coupled into a single-mode fiber for signal examination using a fast photodetector and an electrical spectrum analyzer.

In the literature, optical vortices have been studied in different types of multimode cavities [37,38]. Therefore, benefiting from the rigid structure of the monolithic NPRO, we expect that optical OAM crystals with very narrow linewidths can be generated using NPRO platforms as a result of the superposition of low- and high-order LG modes.

We can theoretically analyze the superposition of amplitude- and phase-locked LG modes in a NPRO. It is well known that LG modes are typical solutions of the paraxial wave equation in cylindrical coordinates. The amplitude distributions can be expressed as [2]

$$\begin{aligned} \mathrm{LG}_{p\ell}(r,z,\phi) = &\sqrt{\frac{2p!}{\pi(p+|\ell|)!}}\frac{1}{w(z)}\left[\frac{r\sqrt{2}}{w(z)}\right]^{|\ell|} \mathrm{L}_p^{|\ell|}\left[\frac{2r^2}{w^2(z)}\right] \\ &\times \exp\left[\frac{-r^2}{w^2(z)}\right]\exp\left[\frac{ik_0 r^2}{2R(z)}\right]\exp(i\ell\phi) \\ &\times \exp\left[-i(2p+|\ell|+1)\arctan\left(\frac{z}{z_R}\right)\right], \end{aligned} \quad (1)$$

where p is the number of nodes of the intensity distribution in the radial direction, ℓ is the topological charge, $w(z)$ is the radius of the beam at z position, w_0 is the beam waist, z_R is the Rayleigh range, and k_0 is the wavenumber. Here $R(z) = (z^2 + z_R^2)/z$ is the curvature of the wavefront, while $\mathrm{L}_p^{|\ell|}$ is the associated Laguerre polynomial. In order to represent the correct intensity distribution for our experimental results, we consider the OAM crystals as the superposition of mode pairs that are both phase and amplitude locked according to: $\psi_A = \alpha \cdot \mathrm{LG}_{00} + \mathrm{LG}_{05}^{+}$ and $\psi_B = \beta \cdot \mathrm{LG}_{01}^{+} + \mathrm{LG}_{06}^{+}$, where ψ_A and ψ_B are the amplitudes for the OAM crystals A and B, and the $+$ sign denotes a positive topological charge, while α and β (set to 0.6 and 0.2, respectively) are the relative phase-locked amplitude ratios.

The calculated intensity patterns at the waist position are shown in Fig. 2. To better understand the formation of OAM crystals, the phase distributions of these modes are presented, together with the intensity distribution. Figures 2(a)–2(c) show the case of OAM crystal A, and one can clearly visualize a phase pattern with the topological charge $\ell = 5$ corresponding to an OAM of $5\hbar$ at the center position. When a fundamental Gaussian beam is superimposed, five spatially distributed OAM crystals are formed as shown. The doughnut-shaped intensity pattern of LG_{05}^{+} then transforms into five zero intensity zones, yielding crystal-like behavior for such OAM crystals. Figures 2(d)–2(f) present the case of the OAM crystal B. Here the superposition of LG_{01}^{+} and LG_{06}^{+} leads to six vortices which are shown in both intensity and phase distribution profiles.

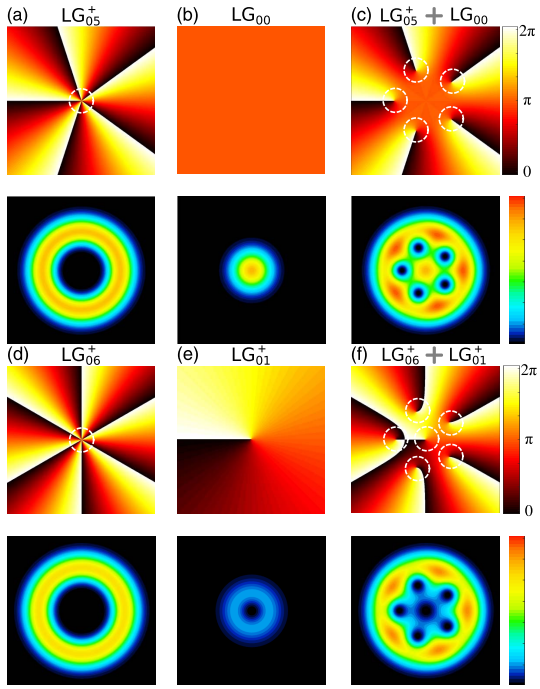

Fig. 2. Calculated phase distribution (top) and intensity distribution (bottom) of different LG modes and the corresponding superposition of these beams leading to the optical OAM crystals A and B. (a) LG_{05}^{+}; (b) LG_{00} or TEM_{00}; (c) optical OAM crystal A: the superposition of LG_{05}^{+} and LG_{00}; (d) LG_{06}^{+}; (e) LG_{01}^{+} and (f) optical OAM crystal B, the superposition of LG_{06}^{+} and LG_{01}^{+}.

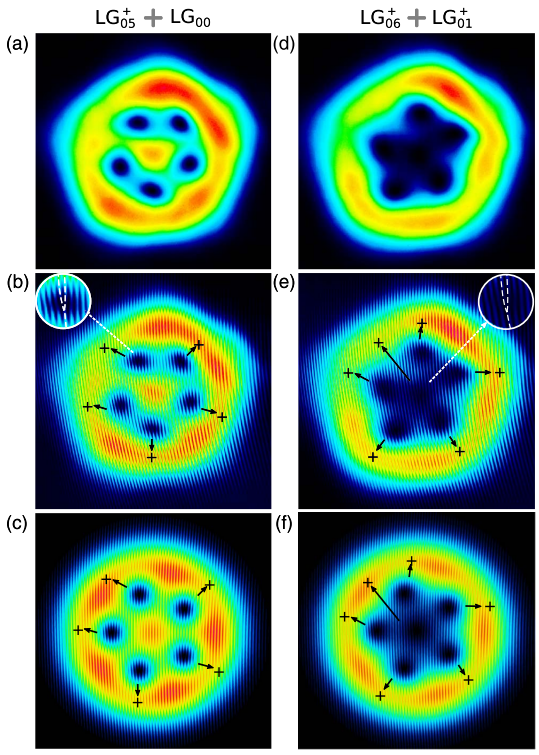

Fig. 3. Experimental intensity output intensity patterns and interference patterns of the optical OAM crystals A and B represented as the superposition of (a) LG_{05}^{+} and (b) LG_{00} and the superposition of (d) LG_{06}^{+} and (e) LG_{01}^{+}. (c) and (f) the corresponding theoretical interference patterns for optical OAM crystals A and B indicating their topological charges or OAMs.

Theoretical calculations have revealed that the superposition of LG modes can lead to interesting particle-like optical OAM crystals. However, a stationary vortex crystal only exists when both amplitude and phase locking occur. For instance, the frequency difference between the component modes would lead to rotating vortices [36]. In a NPRO platform, we have experimentally observed single-frequency lasing featuring optical OAM crystals with five and six stationary vortices. The intensity patterns shown in Figs. 3(a) and 3(d) match the calculated OAM crystals A and B, as presented in Fig. 2. It is interesting to find that these patterns are similar to the vortex states reported in BECs and mesoscopic superconductors [45,51].

Figures 3(b) and 3(e) show the experimental interferograms of the corresponding OAM crystals. It can be observed that each dark intensity regime shows clear dislocated interference fringes that are usually referred to fork-like interferograms. The theoretically calculated interference patterns are also exhibited in Figs. 3(c) and 3(f). They correspond accurately to the experimental recorded fork patterns and evidence positive topological charges. However, we have not observed experimentally OAM crystals with negative topological charges, which we believe could be due to non-phase-locking conditions for those modes.

Using our experimental setup, we were able to monitor the single-frequency behavior of the optical OAM crystal emitters. We could remotely control the pump laser current and record

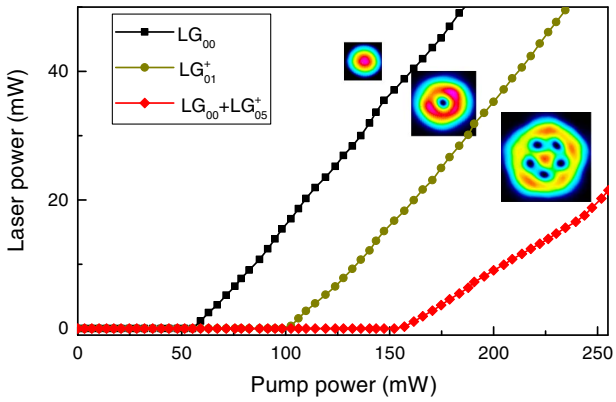

Fig. 4. Comparison of threshold curves for LG_{00}, LG_{01}^{+}, and the vortex crystal $LG_{00} + LG_{05}^{+}$ lasing modes.

the laser threshold data for the OAM crystal A as shown in Fig. 4. Figure 4 shows the recorded threshold curves for three different lasing modes: the fundamental LG mode (LG_{00} or TEM_{00}), the LG_{01}^{+} mode, and the vortex crystal mode ($LG_{00} + LG_{05}^{+}$). The data were recorded with the pump diode driver remotely controlled by a Labview computer program. Simultaneously, the power meter reading was also remotely recorded. The pump driver current was verified by an increment of 5 mA step by step. The program then read 10 sets of data at each step within 2 s, and average values were plotted. Note that error bars were not shown in the figure, as the relative error is less than 1%. One sees that single-frequency vortex crystal lasing (represented by the superposition of LG_{00} and LG_{05}^{+}) was characterized by a high threshold, while the fundamental mode (LG_{00}) has the smallest threshold pump power. The result is dependent on the focused beam size and the incident angle of the pump laser at the Nd:YAG cavity. In fact, the pump Gaussian laser beam is not in perfect overlap with the OAM crystal mode, as can be seen in Fig. 1(b). As a consequence, a slope efficiency of 20% was obtained with a relatively high threshold pump power at 156 mW when compared with the fundamental Gaussian lasing mode in Ref. [41].

We have also investigated the coherence of these laser crystals by monitoring the spectral signature of the photodetected beat notes. A typical single-frequency lasing spectrum acquired from the SFPI is shown in the inset of Fig. 5. To further characterize the laser performance of such single-frequency OAM crystals, the radio frequency (RF) beat note was generated by combining the fiber-coupled laser signal with a commercial NPRO laser (fundamental Gaussian mode) into a fast photodiode. Figure 5 presents the single-tone RF signal obtained from the electrical spectrum analyzer, confirming its single-frequency operation. The 3 dB linewidth (LW) is inferior to 2 kHz (the resolution limit). To the best of our knowledge, this is the best performance reported so far for a free-running optical OAM crystal, and it appears that this high coherence is facilitated by the rigidity of the NPRO platform. It should be noted that a shift of a few tens of micrometers in the relative off-axis position or further increasing pump power could deteriorate its single-frequency operation or cause mode-hopping.

In conclusion, we have reported, to the best of our knowledge, the first observation of optical OAM crystals generated directly in a solid-state monolithic NPRO. The millimeter-size

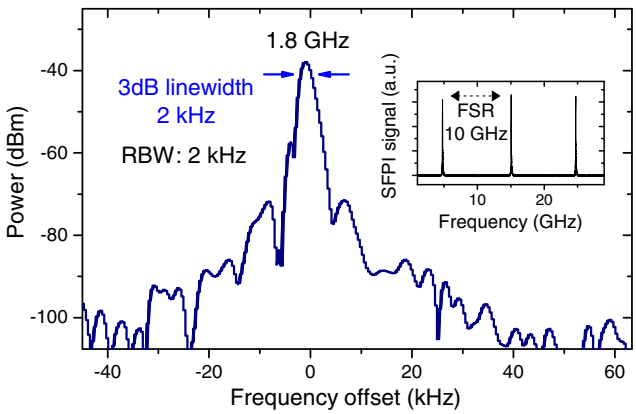

Fig. 5. RF spectra for the photodetected beat notes and SFPI signals (in the inset).

OAM emitter is based on a NPRO made of Nd:YAG crystal and pumped by a single-mode semiconductor Gaussian laser. Thus, the whole system can be considered as rigid and compact. Our finding shows that the narrow-linewidth performance of a Gaussian mode laser is preserved for the OAM beams featuring optical OAM crystals in such NPRO platforms. Considering the fact that NPRO platforms can also emit wavelengths at telecommunication and mid-IR wavelengths depending on the dopant, we expect that our finding can facilitate fundamental studies and applications of complex vortex beams in fields that require highly coherent beams such as large-bandwidth optical communications, precision laser ranging, and spectroscopy.

Funding. National Natural Science Foundation of China (NSFC) (61605051); Fundamental Research Funds for the Central Universities (HUST (2016YXMS014)).

REFERENCES

1. Q. Zhan, Adv. Opt. Photonics **1**, 1 (2009).
2. A. M. Yao and M. J. Padgett, Adv. Opt. Photonics **3**, 161 (2011).
3. M. J. Padgett, Opt. Express **25**, 11265 (2017).
4. L. Allen, M. W. Beijersbergen, R. J. C. Spreeuw, and J. P. Woerdman, Phys. Rev. A **45**, 8185 (1992).
5. A. Mair, A. Vaziri, G. Weihs, and A. Zeilinger, Nature **412**, 313 (2001).
6. A. Vaziri, G. Weihs, and A. Zeilinger, Phys. Rev. Lett. **89**, 240401 (2002).
7. J. Leach, M. J. Padgett, S. M. Barnett, S. Franke-Arnold, and J. Courtial, Phys. Rev. Lett. **88**, 257901 (2002).
8. J. Strohaber, M. Zhi, A. V. Sokolov, A. A. Kolomenskii, G. G. Paulus, and H. A. Schuessler, Opt. Lett. **37**, 3411 (2012).
9. A. Nicolas, L. Veissier, L. Giner, E. Giacobino, D. Maxein, and J. Laurat, Nat. Photonics **8**, 234 (2014).
10. P. Hansinger, G. Maleshkov, I. L. Garanovich, D. V. Skryabin, D. N. Neshev, A. Dreischuh, and G. G. Paulus, Opt. Express **22**, 11079 (2014).
11. D.-S. Ding, W. Zhang, Z.-Y. Zhou, S. Shi, G.-Y. Xiang, X.-S. Wang, Y.-K. Jiang, B.-S. Shi, and G.-C. Guo, Phys. Rev. Lett. **114**, 050502 (2015).
12. N. Schine, A. Ryou, A. Gromov, A. Sommer, and J. Simon, Nature **534**, 671 (2016).
13. A. Aadhi, G. K. Samanta, S. C. Kumar, and M. Ebrahim-Zadeh, Optica **4**, 349 (2017).
14. S. W. Hell and J. Wichmann, Opt. Lett. **19**, 780 (1994).
15. M. Padgett and R. Bowman, Nat. Photonics **5**, 343 (2011).
16. M. Woerdemann, C. Alpmann, M. Esseling, and C. Denz, Laser Photonics Rev. **7**, 839 (2013).
17. C. Hnatovsky, V. G. Shvedov, W. Krolikowski, and A. V. Rode, Opt. Lett. **35**, 3417 (2010).
18. M. Duocastella and C. B. Arnold, Laser Photonics Rev. **6**, 607 (2012).
19. J. Wang, J. Y. Yang, I. M. Fazal, N. Ahmed, Y. Yan, H. Huang, Y. Ren, Y. Yue, S. Dolinar, and M. Tur, Nat. Photonics **6**, 488 (2012).
20. A. E. Willner, H. Huang, Y. Yan, Y. Ren, N. Ahmed, G. Xie, C. Bao, L. Li, Y. Cao, Z. Zhao, J. Wang, M. P. J. Lavery, M. Tur, S. Ramachandran, A. F. Molisch, N. Ashrafi, and S. Ashrafi, Adv. Opt. Photonics **7**, 66 (2015).
21. N. Heckenberg, R. McDuff, C. Smith, and A. White, Opt. Lett. **17**, 221 (1992).
22. M. W. Beijersbergen, L. Allen, H. Van der Veen, and J. Woerdman, Opt. Commun. **96**, 123 (1993).
23. M. Beijersbergen, R. Coerwinkel, M. Kristensen, and J. Woerdman, Opt. Commun. **112**, 321 (1994).
24. X. Cai, J. Wang, M. J. Strain, B. Johnson-Morris, J. Zhu, M. Sorel, J. L. O'Brien, M. G. Thompson, and S. Yu, Science **338**, 363 (2012).
25. R. Barboza, U. Bortolozzo, G. Assanto, E. Vidal-Henriquez, M. G. Clerc, and S. Residori, Phys. Rev. Lett. **109**, 143901 (2012).
26. S. Ngcobo, I. Litvin, L. Burger, and A. Forbes, Nat. Commun. **4**, 2289 (2013).
27. R. Barboza, U. Bortolozzo, G. Assanto, E. Vidal-Henriquez, M. G. Clerc, and S. Residori, Phys. Rev. Lett. **111**, 093902 (2013).
28. E. Karimi, S. A. Schulz, I. De Leon, H. Qassim, J. Upham, and R. W. Boyd, Light: Sci. Appl. **3**, e167 (2014).
29. N. Yu and F. Capasso, Nat. Mater. **13**, 139 (2014).
30. H. Li, D. B. Phillips, X. Wang, Y.-L. D. Ho, L. Chen, X. Zhou, J. Zhu, S. Yu, and X. Cai, Optica **2**, 547 (2015).
31. R. Barboza, U. Bortolozzo, M. G. Clerc, S. Residori, and E. Vidal-Henriquez, Adv. Opt. Photonics **7**, 635 (2015).
32. A. Forbes, A. Dudley, and M. McLaren, Adv. Opt. Photonics **8**, 200 (2016).
33. J. Jimenez-Garcia, P. Rodriguez, T. Guillet, and T. Ackemann, Phys. Rev. Lett. **119**, 113902 (2017).
34. E. Ostrovsky, K. Cohen, S. Tsesses, B. Gjonaj, and G. Bartal, Optica **5**, 283 (2018).
35. M. Brambilla, F. Battipede, L. A. Lugiato, V. Penna, F. Prati, C. Tamm, and C. O. Weiss, Phys. Rev. A **43**, 5090 (1991).
36. M. Vaupel and C. O. Weiss, Phys. Rev. A **51**, 4078 (1995).
37. N. R. Heckenberg, M. Vaupel, J. T. Malos, and C. O. Weiss, Phys. Rev. A **54**, 2369 (1996).
38. J. Scheuer and M. Orenstein, Science **285**, 230 (1999).
39. X. Huang, B. Xu, S. Cui, H. Xu, Z. Cai, and L. Chen, IEEE J. Sel. Top. Quantum Electron. **24**, 1 (2018).
40. S. Wang, S. Zhang, H. Yang, J. Xie, S. Jiang, G. Feng, and S. Zhou, Appl. Phys. Lett. **112**, 201110 (2018).
41. G. Lin, Y. Cao, R. Ji, C. Hou, and Z. Lu, Opt. Lett. **43**, 4164 (2018).
42. B. S. Sheard, G. Heinzel, K. Danzmann, D. A. Shaddock, W. M. Klipstein, and W. M. Folkner, J. Geodes. **86**, 1083 (2012).
43. LIGO collaboration, Phys. Rev. Lett. **116**, 061102 (2016).
44. LISA collaboration, Phys. Rev. Lett. **116**, 231101 (2016).
45. K. W. Madison, F. Chevy, W. Wohlleben, and J. Dalibard, Phys. Rev. Lett. **84**, 806 (2000).
46. A.-C. Ji, W. M. Liu, J. L. Song, and F. Zhou, Phys. Rev. Lett. **101**, 010402 (2008).
47. G. Lin, A. Coillet, and Y. K. Chembo, Adv. Opt. Photonics **9**, 828 (2017).
48. G. Lin, R. Henriet, A. Coillet, M. Jacquot, L. Furfaro, G. Cibiel, L. Larger, and Y. K. Chembo, Opt. Lett. **43**, 495 (2018).
49. G. Lin, R. Martinenghi, S. Diallo, K. Saleh, A. Coillet, and Y. K. Chembo, Appl. Opt. **54**, 2407 (2015).
50. T. J. Kane and R. L. Byer, Opt. Lett. **10**, 65 (1985).
51. H. T. Huy, M. Kato, and T. Ishida, Supercond. Sci. Technol. **26**, 065001 (2013).